Efficiency-Prioritized Droop Control Strategy of AC Microgrid

Yuan, Wenbin; Wang, Yanbo; Liu, Dong; Deng, Fujin; Chen, Zhe

Published in:
IEEE Journal of Emerging and Selected Topics in Power Electronics

DOI (link to publication from Publisher):
10.1109/JESTPE.2020.2967756

Publication date:
2021

Document Version
Accepted author manuscript, peer reviewed version

Efficiency-Prioritized Droop Control Strategy of AC Microgrid

Wenbin Yuan, Yanbo Wang, *Senior Member, IEEE,* Dong Liu, *Senior Member, IEEE,* Fujin Deng, *Senior Member, IEEE,* Zhe Chen, *Fellow, IEEE*

***Abstract*— Operation efficiency is one of important concerns for power conversion system. Efficiency issue of microgrids with multiple paralleled inverters has been paid slightly concerns. Therefore, this paper presents an efficiency analysis method of microgrid in system level and an efficiency-prioritized droop control strategy to improve operation efficiency of microgrids under different load profiles. Efficiency model of microgrid is first established to reveal time-varying efficiency characteristic under different load profiles. Then, optimum solution of efficiency model is derived by Lagrange Multiplier Method, and optimum conditions to capture maximum efficiency are obtained. Furthermore, an efficiency-prioritized droop control strategy is proposed to improve operation efficiency according to the established efficiency model. In addition, stability analysis of the proposed droop controller is performed, from which the guideline for controller design is given. Simulation and experimental results are provided to validate the proposed efficiency-prioritized droop control strategy. The proposed droop control strategy is able to improve overall efficiency of microgrid under different load profiles, which also preserves advantages of conventional droop control strategy.**

***Keywords*—Efficiency-prioritized droop control, adaptive impedance compensation, efficiency model, optimization, paralleled inverters, AC microgrid.**

I. INTRODUCTION

The increasing exploitation of renewable energy sources is promoting development of distributed power generation. The distributed generators (DGs), together with local loads and energy storage devices, can form emerging distributed power generation systems like microgrid and virtual power plant. Microgrid [1]-[2] can be enabled in either grid-connected mode or autonomous mode, which is able to improve reliability and resilience of power supply services [3]-[4].

Operation efficiency is one of important concerns for power conversion system. The efforts toward efficiency improvement for individual inverter have been frequently performed in [5]-[12], where high-efficient modulation methods [5]-[8], topologies design and passive component optimization [9]-[12] are proposed. However, efficiency issue in microgrid with multiple paralleled inverters has been paid very limited concerns. In a paralleled-inverter system, operation efficiency is related with power sharing ratio and load profiles [13]-[17] and it is essential to capture maximum efficiency of microgrids for a long-term energy saving. In fact, the optimum efficiency points are time-varying as variation of load profiles. However, the relationship between optimum operation efficiency and power sharing ratio is slightly investigated in previous works.

Advanced control strategies have been developed to improve operation efficiency of microgrid in previous works [13]-[17]. A dynamic module-dropping strategy is proposed to improve operation efficiency of paralleled inverters under light-load condition in [13], where the number of activated inverters is determined according to load condition. The rest of inverter can be sequentially activated once previous modules reach their maximum output power. However, the efficiency can be further improved by optimizing the number of operated inverters, which has been addressed in [15]-[17]. In [15], a game theoretic-based optimization approach is presented to investigate optimum number of paralleled converters and optimum power sharing ratio in DC microgrids. A forward-backward sweep algorithm is proposed to calculate the optimum power sharing and the optimum switching point for the system with identical inverters in [16]. Similar analysis for microgrid with multiple paralleled inverters is implemented in [17]. However, the application of centralized communication facilities mitigates reliability and increases system cost [18]-[19].

Several efforts have been made to improve system efficiency by dynamically regulating power sharing ratio [20]-[22],[27]. A hierarchical control strategy is developed to improve efficiency of DC microgrids in [20], where genetic algorithm is applied to capture optimum efficiency points and an adaptive virtual resistance (VR) controller is developed to track the optimum efficiency point. A smart control strategy is proposed to enhance conversion efficiency of paralleled inverters at light loads in [21], where particle swarm optimization algorithm is implemented to calculate current references of paralleled inverters for optimum system efficiency. An exhaustive optimization-based control strategy is developed in [22] to improve operation efficiency of wind energy conversion system. However, centralized communication channel is required in [20]-[22] to implement the optimization procedure, which undoubtedly increases operation cost, and mitigates reliability of microgrid due to side effects such as data drop-out and time delay [23]-[26]. To deal with the drawbacks, a

This work was supported by the ForsKEL and EUDP project "Voltage control and protection for a grid towards 100% power electronics and cable network (COPE)" (No. 880063).

Wenbin Yuan, Yanbo Wang, Dong Liu and Zhe Chen are with the Department of Energy Technology, Aalborg University, Aalborg 9220, Denmark (e-mail: wyu@et.aau.dk; ywa@et.aau.dk; dli@et.aau.dk; zch@et.aau.dk). (*Corresponding author: Yanbo Wang.*)

Fujin Deng is with the School of Electrical Engineering, Southeast University, Nanjing 210096, China (e-mail: fdeng@seu.edu.cn).

distributed communication-based control strategy is proposed to improve operation efficiency of microgrid by adjusting power sharing ratio in [27], where a dynamic consensus algorithm is applied to solve optimization problem according to information from neighbors. However, the optimum sharing ratio is obtained by real-time online computation, which tends to increase computational burdens. The main drawbacks of existing work are summarized as follows. (1) Mathematical model for efficiency analysis and optimization are slightly concerned, which is important to analyze and optimize efficiency of microgrid. (2) Effect of reactive power allocation on system efficiency has not been analyzed. (3) For existing control strategies, communication facilities are required to implement efficiency improvement, which mitigates reliability and flexibility of control system. (4) The efforts toward efficiency improvement in droop-controlled microgrid are merely performed.

Therefore, this paper presents an efficiency-prioritized droop control strategy to improve operation efficiency of microgrid without using communication facilities as an extension of our previous conference work [28]. Main contributions of this paper are explained as follows. (1) Unified efficiency model is established to reveal efficiency characteristic of microgrids under time-varying active and reactive load profiles. (2) Efficiency optimization method is developed where the optimization problem is solved by taking advantage of Lagrange Multiplier Method. (3) Efficiency-prioritized droop control strategy with dynamic impedance compensation loop is developed, which is able to improve operation efficiency of microgrids according to the established efficiency optimization method. (4) Stability of the proposed controller is analyzed, from which the guideline for controller parameters is formulated.

The rest of this paper is organized as follows. In Section II, conventional droop control strategy is reviewed. In Section III, efficiency model of microgrid is established to reveal the relationship between system efficiency and load profiles. Also, operation conditions to capture maximum efficiency point are derived by Lagrange Multiplier Method. In Section IV, the efficiency-prioritized droop control strategy with adaptive impedance compensation loop is proposed, where basic principle and implementation procedure is given according to derived optimum operation conditions. In addition, stability analysis is performed to formulate guideline for parameters of the proposed controller. In Section V and VI, simulation and experimental results are provided to validate effectiveness of the proposed efficiency-prioritized droop control strategy. Conclusions are drawn in Section VII.

II. System Description and Problem Formulation

Fig. 1 shows circuit configuration of an islanded microgrid with N-paralleled inverters, where droop control strategy is applied to implement proportional power sharing without using critical communication facilities. The classical active power-frequency (P-ω) and reactive power-voltage (Q-V) droop control strategy [29] can be given as (1)-(2).

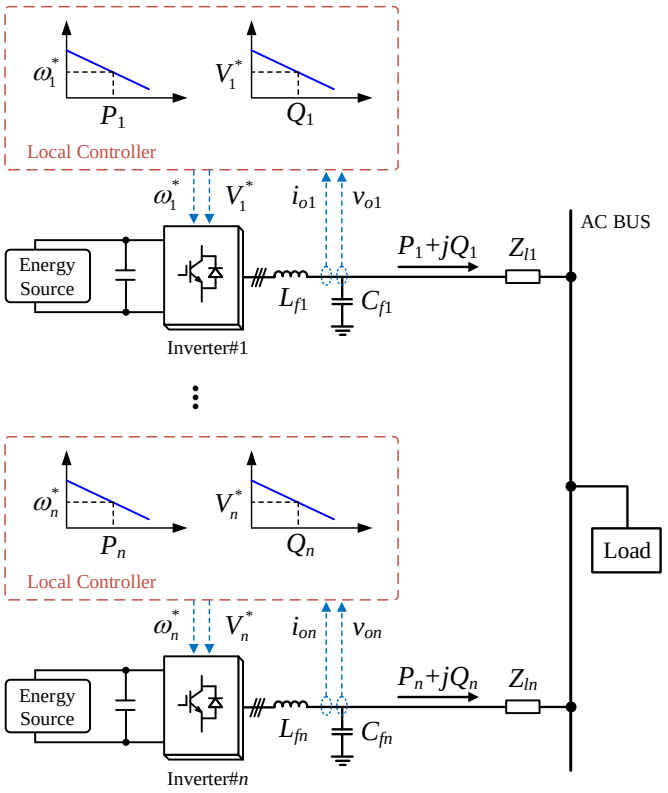

Fig. 1. Circuit configuration of islanded AC microgrid.

$$\omega_i^* = \omega_0 - m_i P_i,\ m_i = (\omega_{\max} - \omega_{\min}) / P_{\max i} \quad (1)$$

$$V_i^* = V_0 - n_i Q_i,\ n_i = (V_{\max} - V_{\min}) / Q_{\max i} \quad (2)$$

where ω_i^* and V_i^* are reference commands of angular frequency and output voltage amplitude. P_i and Q_i are output active and reactive power of i-th inverter. $P_{\max i}$ and $Q_{\max i}$ are active and reactive power ratings of i-th inverter. ω_0 and V_0 are angular frequency and output voltage of inverter without load. m_i and n_i are power rating-dependent droop coefficients of i-th inverter. $\omega_{\max}$ and $\omega_{\min}$ are maximum and minimum values of allowable angular frequency. $V_{\max}$ and $V_{\min}$ are maximum and minimum values of allowable voltage amplitude.

Power sharing relationship of paralleled inverters is derived from (1) and (2) as (3).

$$\begin{cases} P_1 / P_2 = m_2 / m_1 = P_{\max 1} / P_{\max 2} \\ Q_1 / Q_2 = n_2 / n_1 = Q_{\max 1} / Q_{\max 2} \end{cases} \quad (3)$$

It can be seen from (3) that conventional droop control strategy can perform proportional power sharing according to active and reactive power ratings of inverters.

Fig. 2 shows power loss (P_{loss}) characteristic with respect to output active power and reactive power of inverter1 and inverter2, and parameters of power devices are given in Table I. Fig. 2(b) shows P_i-P_{loss} characteristic with Q_i=0 and Fig. 2(c) shows Q_i-P_{loss} characteristic with P_i=0. It can be seen that power loss of inverter is changed as variation of output active power and reactive power. In addition, different power devices have different power loss characteristics, which can thus change optimum efficiency points. Taking 90% load condition

in Fig. 2(b) as an example, inverters will work at operation points A and B under conventional droop control strategy. However, system efficiency can be improved by tuning operation point of inverter1 to A' and adjusting operation point of inverter2 to B', because the reduced power loss in inverter1 ΔP_{loss1} is larger than increased power loss in inverter2 ΔP_{loss2}, resulting in improved operation efficiency. In addition, Fig. 3 shows theoretically estimated efficiency curves with different power sharing ratios (K_P=P_1/P_2, K_Q=Q_1/Q_2) under various load profiles, where the red-solid line is the system efficiency curve under conventional droop control (K_P=1, K_Q=1) and the green-dotted line is the optimum system efficiency curve. The efficiency curves shown in Fig. 3 illustrate that the optimum efficiency points are time-varying as variation of load profiles and the optimum efficiency point is related with the steady-state power sharing ratios K_P and K_Q. However, conventional droop control strategies fail to implement optimum efficiency control. Therefore, the aim of this paper is to investigate time-varying efficiency characteristic of microgrid and develop an efficiency-prioritized droop control strategy for system efficiency improvement.

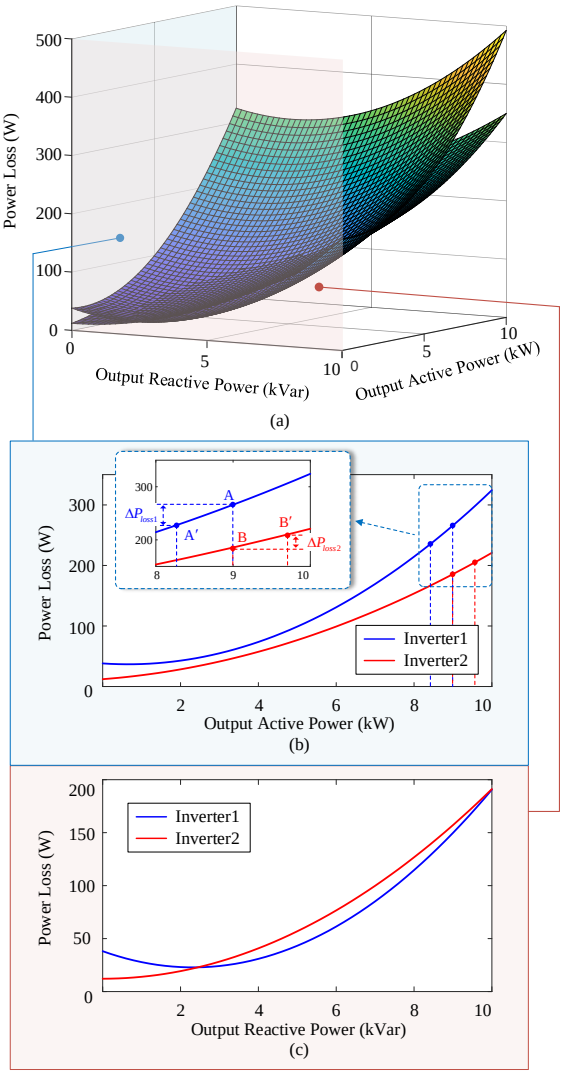

Fig. 2. Power loss characteristics of inverters.

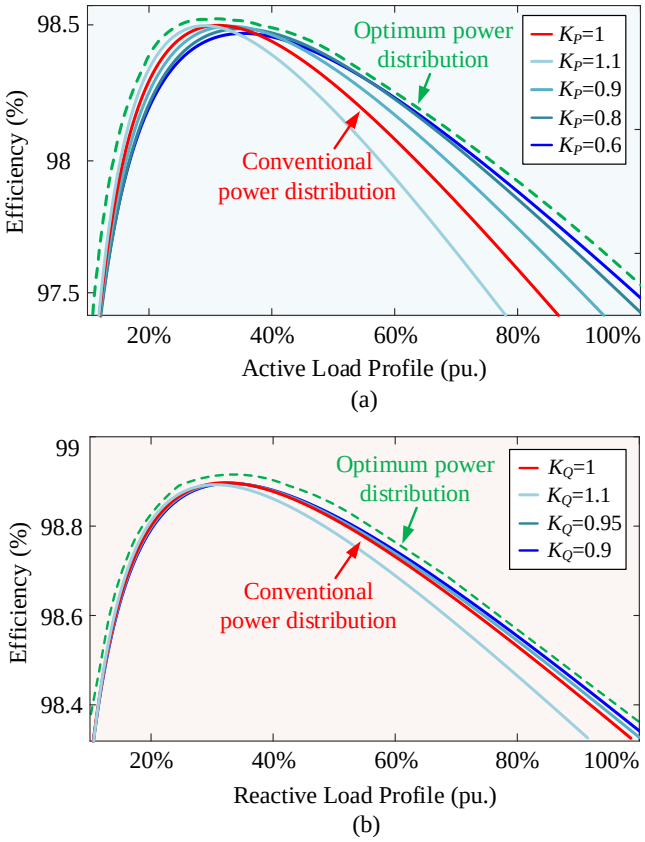

Fig. 3. Theoretical system efficiency curves with different power sharing ratios.

III. Proposed Efficiency Modelling and Analysis Method of Microgrid

In this section, efficiency model of microgrid is first established under time-varying active and reactive power loads. Then, the optimum operation conditions of efficiency model are derived by Lagrange Multiplier Method.

Power loss characteristic of i-th inverter can be fitted as a function of output active power and reactive power as (4) [16].

$$P_{loss\_i} = a_i P_i^2 + b_i P_i + c_i Q_i^2 + d_i Q_i + e_i P_i Q_i + h_i \quad (4)$$

where a_i, b_i, c_i, d_i, e_i and h_i are coefficients in fitted function, which can be obtained by fitting experimental data.

For a microgrid with N-paralleled inverters, system efficiency can be defined as (5).

$$\eta_{sys} = \frac{P_{load}}{P_{load} + P_{loss\_tot}} \quad (5)$$

where

$$P_{loss\_tot} = \sum_{i=1}^{N} P_{loss\_i} \quad (6)$$

Since the load demand is fixed in steady state, the system efficiency is optimal under minimum power loss. Therefore, the optimization problem without consideration of power ratings can be formulated as (7).

$$\min\left(P_{loss\_tot}\right)$$
$$s.t.\begin{cases}\sum_{i=1}^{N}P_i = P_{load}\\ \sum_{i=1}^{N}Q_i = Q_{load}\end{cases} \quad (7)$$

The Lagrange function is established to derive the optimal solution as (8).

$$L = P_{loss\_tot} + \lambda_1\left(P_{load} - \sum_{i=1}^{N}P_i\right) + \lambda_2\left(Q_{load} - \sum_{i=1}^{N}Q_i\right) \quad (8)$$

where λ_1 and λ_2 are Lagrange multipliers. And the optimum solution can be obtained by solving (9).

$$\begin{cases}\frac{\partial L}{\partial P_1}=0,\ \frac{\partial L}{\partial P_2}=0,\ \ldots,\ \frac{\partial L}{\partial P_n}=0\\ \frac{\partial L}{\partial Q_1}=0,\ \frac{\partial L}{\partial Q_2}=0,\ \ldots,\ \frac{\partial L}{\partial Q_n}=0\\ \frac{\partial L}{\partial \lambda_1}=P_{load}-\sum_{i=1}^{N}P_i=0\\ \frac{\partial L}{\partial \lambda_2}=Q_{load}-\sum_{i=1}^{N}Q_i=0\end{cases} \quad (9)$$

In order to investigate optimum conditions of maximum efficiency, necessary conditions of the optimum solution are given as (10) by simplifying (9).

$$\begin{cases}\frac{\partial P_{loss\_1}}{\partial P_1}=\frac{\partial P_{loss\_2}}{\partial P_2}=\cdots=\frac{\partial P_{loss\_n}}{\partial P_n}\\ \frac{\partial P_{loss\_1}}{\partial Q_1}=\frac{\partial P_{loss\_2}}{\partial Q_2}=\cdots=\frac{\partial P_{loss\_n}}{\partial Q_n}\end{cases} \quad (10)$$

Equation (10) reveals the relationship between optimum operation efficiency and active/reactive power sharing. In addition, some connotations can be drawn from (10). (1) For a microgrid with identical inverters, the optimum output powers of inverters are equal due to similarity of power loss characteristics of inverters. (2) For a microgrid with different inverters, the optimum power sharing ratio is related with power loss characteristics of inverters. And the optimum power sharing ratio is time-varying as variation of load profiles, which agrees with the efficiency curves as shown in Fig. 3.

IV. Proposed Efficiency-Prioritized Droop Control Strategy

In this section, an efficiency-prioritized droop control strategy is developed to optimize operation efficiency of microgrid according to the efficiency model established in Section III. A microgrid with two inverters is applied to exemplify the proposed droop controller. In the two inverters, different power devices are applied, whose parameters are given in Table I in Section V.

Fig. 4 shows diagram of the proposed droop controller. Power loss coefficients of each inverter are computed according to the power loss model established in Section III by off-line calculation. Then, these coefficients are incorporated into local adaptive droop controller to perform the optimum active power sharing. And a dynamic impedance compensation loop is added to reshape output impedance of inverter, resulting in the optimum reactive power sharing. It can be seen from Fig. 4 that the proposed controller is implemented without using communication facilities, which thus enhance reliability and flexibility of power control system.

A. Adaptive P-ω droop control strategy for optimum efficiency control

In order to perform optimum efficiency control, adaptive *P-ω* droop control strategy is developed according to the first necessary condition (10), which is given as (11).

$$\begin{cases}\omega_i^* = \omega_{0i}' - m_i' P_i\\ \omega_{0i}' = \omega_0 - k_P\left(b_i + e_i Q_i\right)\\ m_i' = 2k_P a_i\end{cases} \quad (11)$$

where ω_{0i}', V_{0i}', m_i' and n_i' are retuned droop parameters that are related with power loss coefficients of each inverter. k_P is a constant which should be designed for avoiding large frequency deviation.

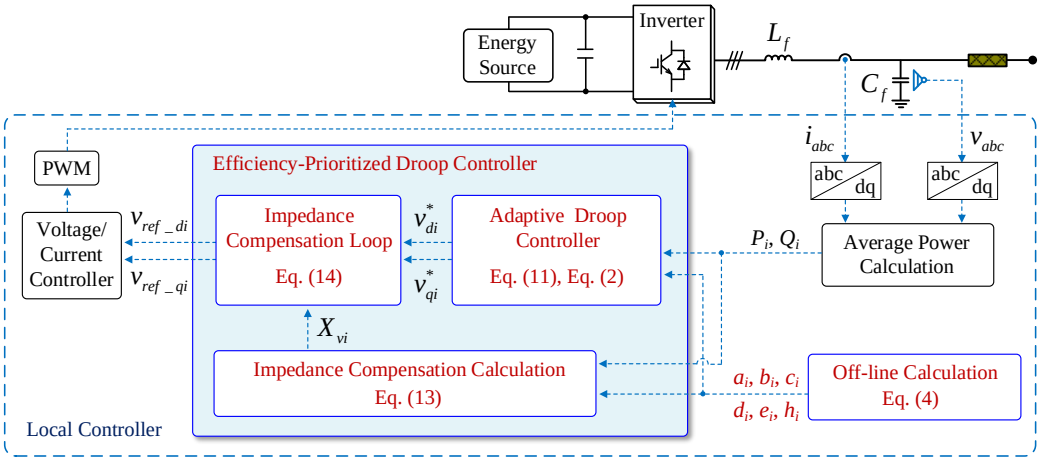

Fig. 4. The block diagram of proposed efficiency-prioritized droop controller.

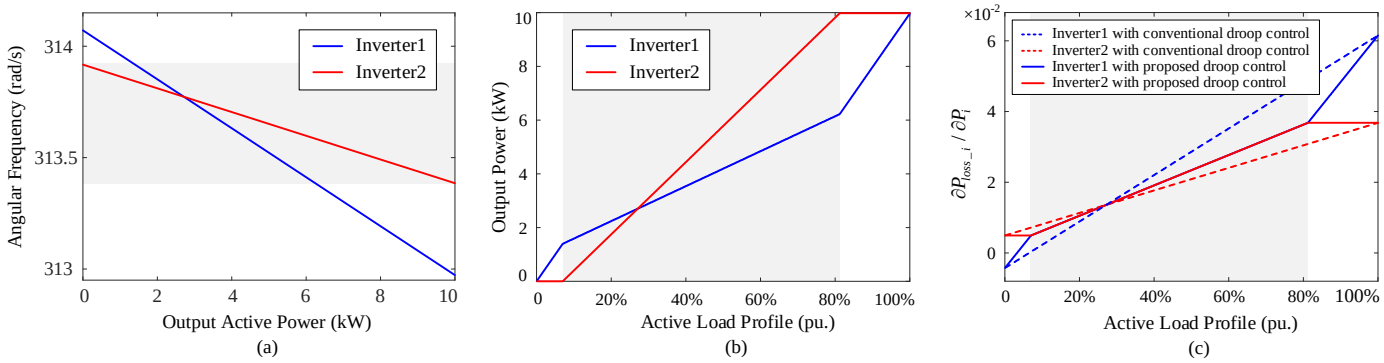

Fig. 5. Performance of proposed *P-ω* droop controller. (a) *P-ω* droop curves. (b) Power sharing characteristic under different active load profiles. (c) $\partial P_{loss\_i}/\partial P_i$ under different active load profiles.

The power relationship of inverter1 and inverter2 can be obtained by (11) as (12) in steady state.

$$2a_1P_1 + b_1 + e_1Q_1 = 2a_2P_2 + b_2 + e_2Q_2 \tag{12}$$

Combining (4) and (12), the first term in (10) is obtained, which indicates the optimum condition with respect to active power sharing for maximum system efficiency is satisfied by the proposed droop control strategy.

Fig. 5 shows retuned *P-ω* droop curves and performance of the proposed droop controller with time-varying active load, where the power sharing characteristic of paralleled inverters is shown in Fig. 5(b). Fig. 5(c) shows partial derivative of power loss with respect to output active power under time-varying active load profiles. It can be seen that optimum condition (10) can be satisfied under most of the load demand (7%—81% in this case).

B. Reactive power sharing control for optimum efficiency control

It is well-known that the accuracy of reactive power sharing is affected by output impedances of inverters [26]. In order to perform optimum efficiency control, a nonlinear impedance compensation loop is given as (13) to reshape equivalent output impedances of inverters according to the second necessary condition in (10).

$$\begin{cases} X_{vi} = X_{oi}^{*} - X_{oi} \\ X_{oi}^{*} = \left(2c_i + \dfrac{d_i + e_i P_i}{Q_i}\right) k_Q \end{cases} \tag{13}$$

where X_{oi} is closed-loop output impedance of the *i*-th inverter whose details can be found in [30]. X_{oi}^{*} is the equivalent fundamental impedance. k_Q is a constant which is equal for all inverters.

Reference voltage incorporating nonlinear impedance compensation loop is given as (14).

$$\begin{cases} v_{ref\_di} = v_{di}^{*} + X_{vi} i_{oqi} \\ v_{ref\_qi} = v_{qi}^{*} - X_{vi} i_{odi} \end{cases} \tag{14}$$

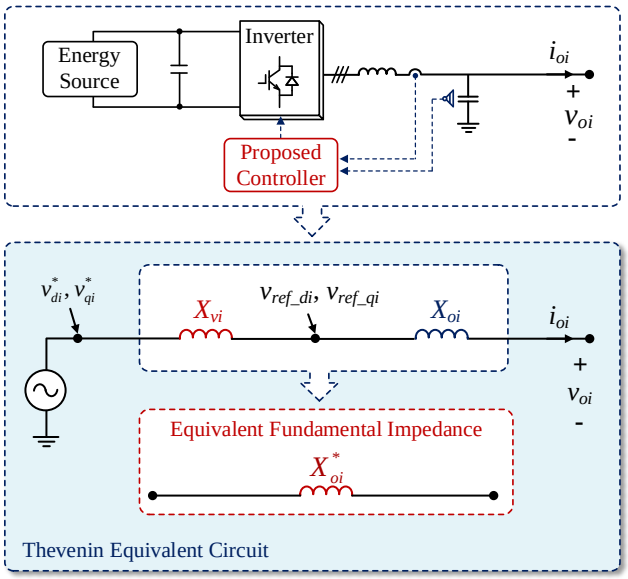

Fig. 6. Thevenin equivalent circuit of inverter with impedance compensation loop.

where v_{di}^{*} and v_{qi}^{*} are original voltage references derived from droop control method, i_{odi} and i_{oqi} are inverter output current in *dq* frame. v_{ref_di} and v_{ref_qi} are updated voltage references in *dq* frame obtained from impedance compensation loop.

Fig. 6 shows Thevenin equivalent circuit of inverter with impedance compensation loop. Then, the reactive power sharing ratio of inverters with the proposed impedance compensation method can be given as (15) [30],[31].

$$\frac{Q_1}{Q_2} = \frac{X_{o2} + X_{v2} + X_{l2} + n_2 V_p}{X_{o1} + X_{v2} + X_{l1} + n_1 V_p} = \frac{X_{o2}^{*} + X_{l2} + n_2 V_p}{X_{o1}^{*} + X_{l1} + n_1 V_p} \tag{15}$$

where X_{li} is line impedance between the *i*-th inverter and the point of common coupling (PCC). V_P is voltage amplitude at PCC. X_{oi}^{*} is equivalent fundamental impedance which can be dynamically tuned according to power loss coefficients and output power of the *i*-th inverter.

By tuning the coefficient k_Q in (13), $X_{oi}^{*} \gg (X_{li} + n_i V_p)$ can be ensured. Then, reactive power sharing is mainly determined by X_{oi}^{*} as (16), so that (17) can be obtained in steady state.

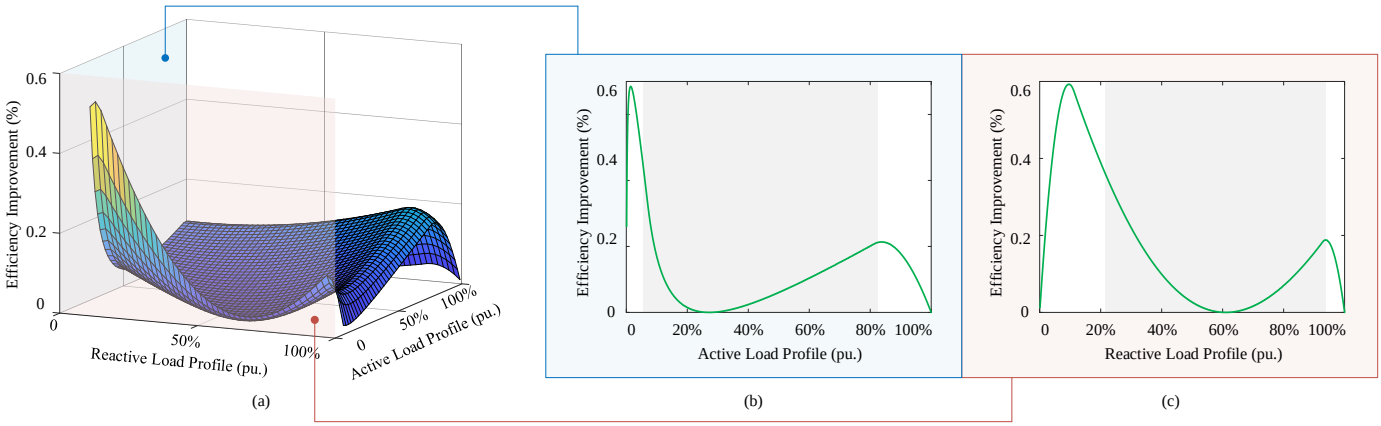

Fig. 7. Efficiency improvement compared with conventional droop control.

$$\frac{Q_1}{Q_2}=\frac{X_{o2}^*}{X_{o1}^*}=\frac{2c_2+\dfrac{d_2+e_2P_2}{Q_2}}{2c_1+\dfrac{d_1+e_1P_1}{Q_1}} \tag{16}$$

$$2c_1Q_1+d_1+e_1P_1=2c_2Q_2+d_2+e_2P_2 \tag{17}$$

The second term in (10) is obtained by combining (4) and (17), which indicates the optimum condition with respect to reactive power for maximum system efficiency is satisfied automatically with the proposed impedance compensation method.

Fig. 7 shows theoretical system efficiency improvement under the proposed efficiency-prioritized droop control strategy as variation of load profiles, where the improved efficiency η_{imp} is defined as (18).

$$\eta_{\text{imp}}=\frac{\eta_{\text{pro}}-\eta_{\text{con}}}{\eta_{\text{con}}}\cdot 100\% \tag{18}$$

where η_{con} and η_{pro} are efficiency under conventional droop control and proposed droop control. It can be seen that the overall efficiency can be improved within a wide load profile.

C. Small signal modelling of the proposed efficiency-prioritized droop control strategy

In this section, small signal model of microgrids with proposed efficiency-prioritized droop control strategy is first established. And stability analysis is then implemented.

Small signal equation of the proposed efficiency-prioritized droop controller can be obtained as (19) by combining and linearizing (11), (13) and (14).

$$\begin{bmatrix}\Delta\omega_i^*\\ \Delta v_{ref\_di}\\ \Delta v_{ref\_qi}\end{bmatrix}=A_{1\omega vi}\begin{bmatrix}\Delta\delta_i\\ \Delta P_i\\ \Delta Q_i\end{bmatrix}+A_{2\omega vi}\begin{bmatrix}\Delta i_{odi}\\ \Delta i_{oqi}\end{bmatrix} \tag{19}$$

where

$$\begin{cases} A_{1\omega vi}=\begin{bmatrix}0 & -2k_Pa_i & -k_Pe_i\\ 0 & i_{oqi\_0}K_{X_{vi}\_P_i} & i_{oqi\_0}K_{X_{vi}\_Q_i}-n_i\\ 0 & -i_{odi\_0}K_{X_{vi}\_P_i} & -i_{odi\_0}K_{X_{vi}\_Q_i}\end{bmatrix}\\ A_{2\omega vi}=\begin{bmatrix}0 & 0\\ 0 & X_{vi\_0}\\ -X_{vi\_0} & 0\end{bmatrix}\\ K_{X_{vi}\_P_i}=\left.\dfrac{\partial X_{vi}}{\partial P_i}\right|_{P_{i\_0},Q_{i\_0}},\ K_{X_{vi}\_Q_i}=\left.\dfrac{\partial X_{vi}}{\partial Q_i}\right|_{P_{i\_0},Q_{i\_0}}\end{cases} \tag{20}$$

where P_{i_0}, Q_{i_0}, i_{odi_0} and i_{oqi_0} are initial values of output active power, reactive power and current of the i-th inverter at steady-state operating point. X_{vi_0} is impedance compensation value under P_{i_0} and Q_{i_0}.

Details of voltage/current controller, network and load models can be found in [32]-[34]. On the basis of this, small signal dynamics of the proposed power controller, network and load can be represented in common DQ frame as (21).

$$\Delta\dot{x}=A\Delta x \tag{21}$$

where Δx is the vector of state variables of the system, which is shown in (22). A is the system parameter matrix, which is given in Appendix.

$$\begin{cases}\Delta x=\begin{bmatrix}\Delta x_{inv1} & \Delta x_{inv2} & \cdots & \Delta x_{invN} & \Delta i_{lineDQi} & \Delta i_{loadDQi}\end{bmatrix}^T\\ \Delta x_{invi}=\begin{bmatrix}\Delta\delta_i & \Delta P_i & \Delta Q_i & \Delta i_{odqi}\end{bmatrix}^T\end{cases} \tag{22}$$

D. Small signal stability analysis

Small signal stability of microgrid with the proposed efficiency-prioritized droop control is analyzed by investigating eigenvalue trace of state matrix A on the basis of parameters of inverter1 and inverter2 given in Table I. Fig. 8 shows dominant poles as variation of parameter k_P. It can be seen that λ_1 and λ_2 move toward right half-plane as increase of k_P, where the critical value of stability region is 4.5e2. Meanwhile, damping ratio of system is decreased as increase of k_P, improving system dynamic response. Fig. 8 shows that k_P has critical influence on system stability and dynamic

performance. In addition, k_P should be limited as (23) for avoiding large frequency deviation.

$$k_P = \min\left(k_{P1\_\max}, k_{P2\_\max}, \cdots, k_{Pn\_\max}\right) \tag{23}$$

where

$$k_{Pi\_\max} = \frac{\Delta\omega_{\max}}{b_i + e_i Q_{\max i} + 2a_i P_{\max i}} \tag{24}$$

Considering frequency droop limitation ($\Delta\omega_{\max}$=0.4%·ω_0) and system dynamic performance, desirable operation region of k_P is given as k_P∈[1, 19.9].

Fig. 9 shows dominant poles as variation of parameter k_Q. It can be seen that all the dominant poles lie on the left of the imaginary axis as increase of k_Q, remaining system stable. While damping ratio of system is increased as increase of k_Q, slowing down system dynamic response. Therefore, considering voltage droop limitation (less than 10%), reactive power sharing performance and system dynamic performance, desirable operation region of k_Q is given as k_Q∈[1e4, 5e5].

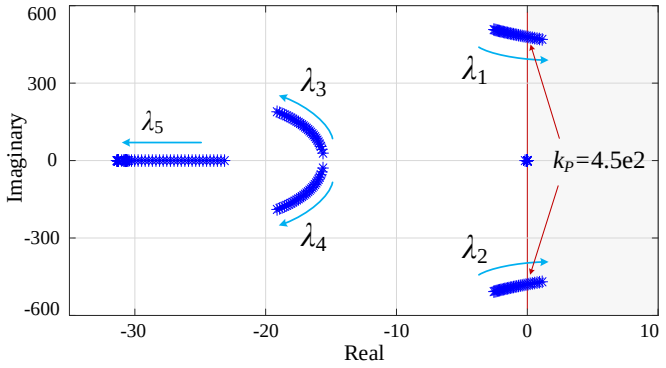

Fig. 8. Dominant poles as k_P∈[0.1, 4.7e2].

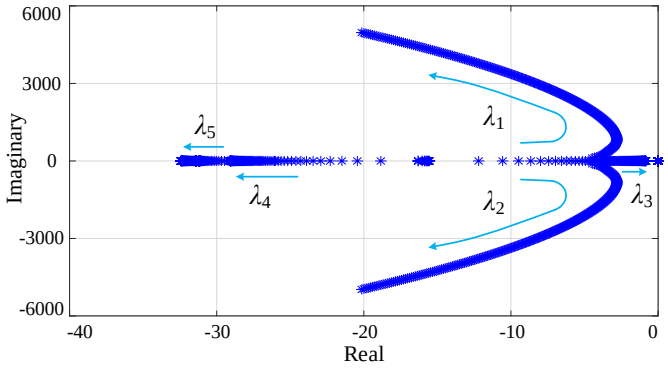

Fig. 9. Dominant poles as k_Q∈[0, 1e6].

V. Simulation Verification

To validate effectiveness of the proposed efficiency-prioritized droop control strategy, simulation verification is implemented in a scale-down AC microgrid with two inverters in MATLAB with PLECS blockset. Circuit configuration of the exemplified microgrid is shown in Fig. 1. The simulation parameters are given in Table I. The detailed parameters of power devices can be seen in datasheets [35]-[37].

TABLE I
System Parameters in Simulation

Inverter Parameters			
	Inverter1	Inverter2	Inverter3
Manufacturer	Infineon	Semikron	Semikron
Power device	FS6R06VE3_B2	SKiiP 01NEC066V3	SK30GD066 ETp
Rated maximum power	P_{max1}=10kW Q_{max1}=10kVar	P_{max2}=10kW Q_{max2}=10kVar	P_{max3}=30kW Q_{max3}=30kVar
DC voltage	V_{dc1}=600V	V_{dc2}=600V	V_{dc3}=600V
Power loss coefficients	a_1=3.29e-6 b_1=-4.28e-3 c_1=2.84e-6 d_1=-1.32e-2 e_1=1.54e-7 h_1=38.14	a_2=1.59e-6 b_2=4.94e-3 c_2=1.79e-6 d_2=1.49e-5 e_2=-5.02e-7 h_2=12.14	a_3=2.33e-7 b_3=5.38e-3 c_3=2.32e-7 d_3=6.42e-3 e_3=-2.13e-7 h_3=28.38
Circuit and Control Parameters			
Filter parameters	L_{f1}= L_{f3}=4mH C_{f1}= C_{f3}=50μF L_{f2}=2mH C_{f2}=25μF	Phase voltage frequency reference	V_m^*=311V ω^*=100π rad/s
Line impedance	Z_{l1}=(0.1+j0.63) Ω Z_{l2}= Z_{l3}= (0.15+j1.26) Ω	Switching frequency	f_{sw1}= f_{sw2}= f_{sw3}=10kHz
Adaptive droop coefficient	k_P=15	Impedance compensation coefficient	k_Q=2e5

Case I: Inverters with same power devices

In this case, operation performance of paralleled-inverters with same power devices (FS6R06VE3_B2) under proposed droop controller is tested. Fig. 10 shows simulation results about active and reactive power sharing under conventional droop control strategy and the proposed droop control strategy. It can be seen from Fig. 10(a)-(d) that the proposed droop control strategy, similar with conventional droop control strategy, can implement equal active and reactive power sharing. Fig. 10(e) shows steady-state efficiency of microgrid with conventional droop controller and proposed droop controller. It can be seen that operation efficiency under proposed droop control method is identical with efficiency under conventional droop control strategy. These simulation results agree with the theoretical analysis in Section III.

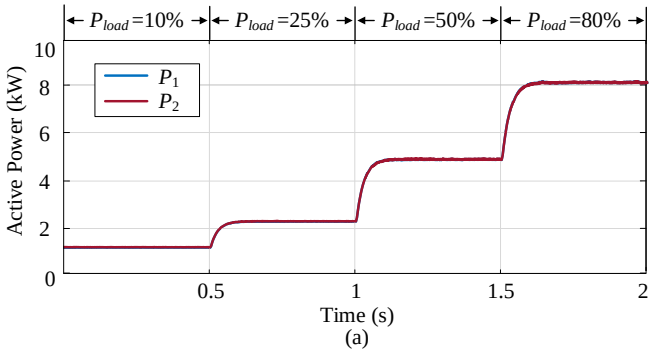

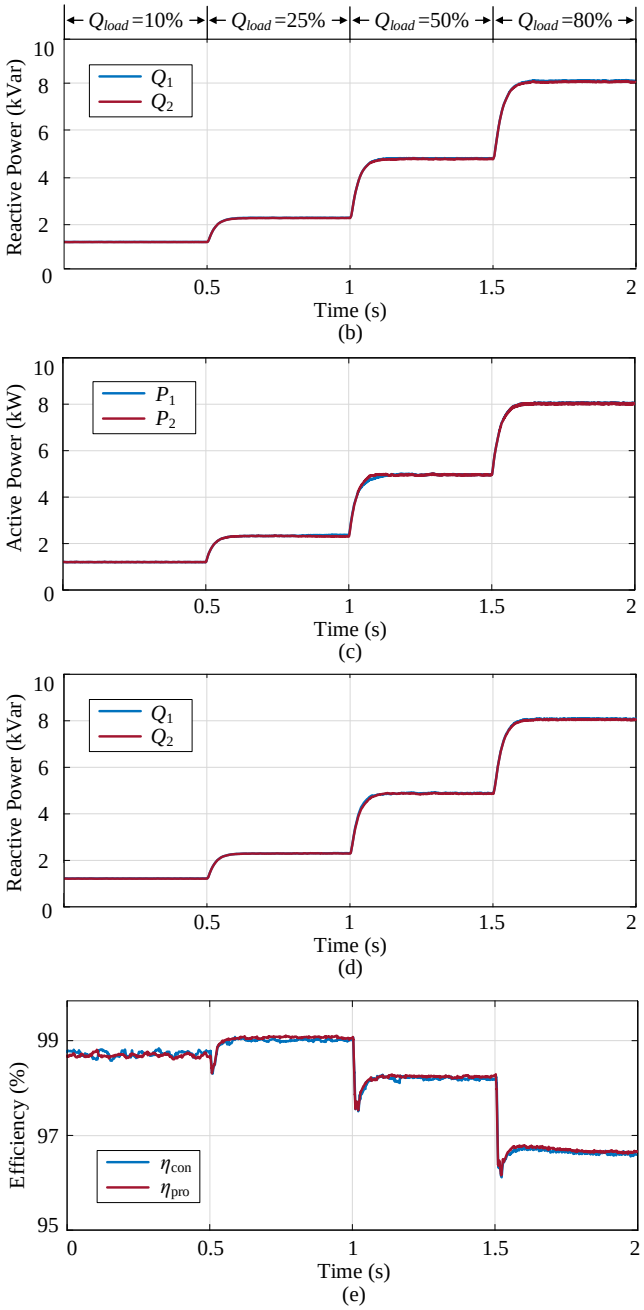

Fig. 10. Simulation results of case I. (a) Active power sharing under conventional droop control strategy. (b) Reactive power sharing under conventional droop control strategy. (c) Active power sharing under proposed droop control strategy. (d) Reactive power sharing under proposed droop control strategy. (e) System efficiency under conventional and proposed droop control strategy.

Case II: Inverters with different power devices

Fig. 11 shows simulation results of paralleled inverters with same power ratings but different power devices (FS6R06VE3_B2 and SKiiP 01NEC066V3). In order to analyze efficiency characteristic of microgrid under different load profiles, time-varying load is exerted as 10% system capacity during 0-0.5s, 25% system capacity during 0.5-1s, 50% system capacity during 1-1.5s and 80% system capacity during 1.5-2s. Fig. 11(a)-(b) show power sharing characteristics under conventional droop control strategy. Fig. 11(c)-(d) show power sharing characteristics under proposed efficiency-prioritized droop control strategy. It can be seen that different with conventional droop control method, the power sharing ratio under proposed droop control strategy is regulated adaptively as variation of load profiles for optimum system efficiency. Fig. 11(e) shows that impedance compensation values are dynamically tuned to adjust reactive power sharing according to condition of optimum operation efficiency. Also, It can be seen that the proposed control method is able to ensure desirable transient responses during load step.

Fig. 11(f) shows comparison analysis of system efficiency under conventional droop control and proposed droop control. It can be seen that system efficiency is obviously improved by 0.23%, 0.18%, 0.17% and 0.27% under 10%, 25%, 50% and 80% system capacity. The result of improved efficiency is shown in Table II. These simulation results agree with theoretical analysis as shown in Fig. 5 and Fig. 7.

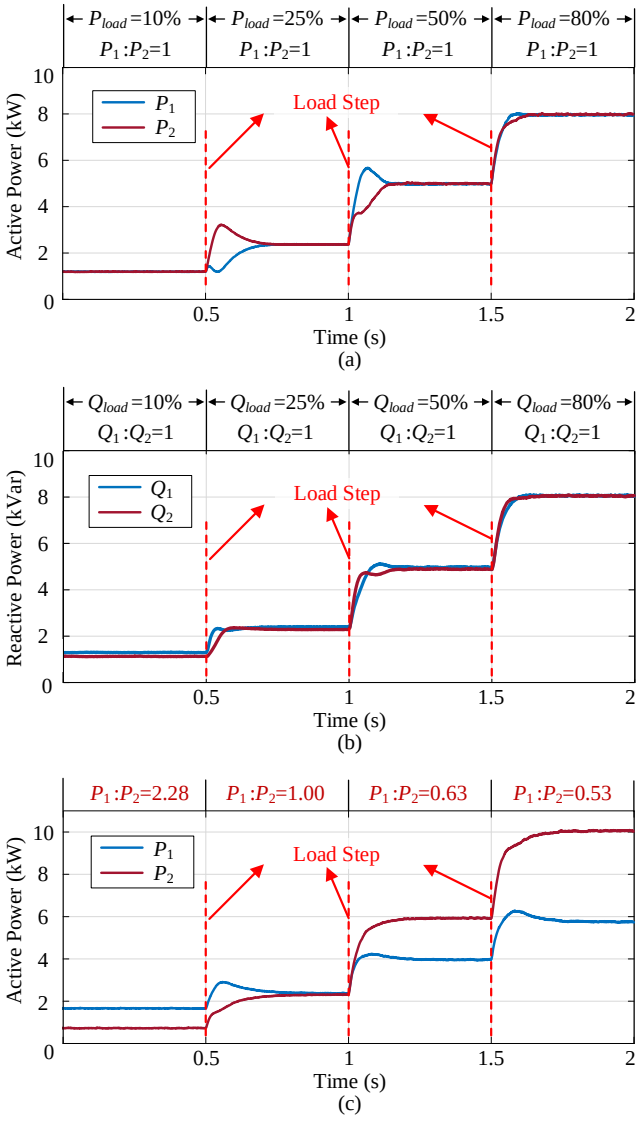

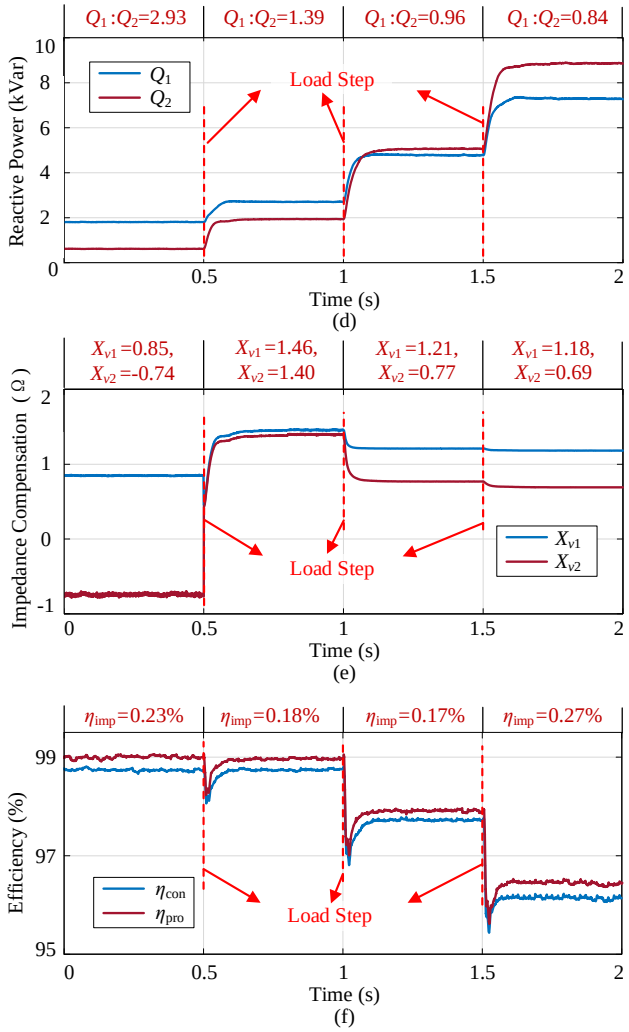

Fig. 11. Simulation results of case II. (a) Active power sharing under conventional droop control strategy. (b) Reactive power sharing under conventional droop control strategy. (c) Active power sharing under proposed droop control strategy. (d) Reactive power sharing under proposed droop control strategy. (e) Dynamic impedance compensation values. (f) System efficiency under conventional and proposed droop control strategy.

TABLE II
RESULTS ABOUT IMPROVED EFFICIENCY IN SIMULATION

Case II				
Load Profiles	10%	25%	50%	80%
η_{imp}	0.23%	0.18%	0.17%	0.27%
Case IV				
Load Profiles	10%	20%	50%	80%
η_{imp}	0.25%	0.27%	0.15%	0.46%

Case III: Inverters with different control parameters

To further validate effectiveness of the parameter region proposed in Section IV, simulation validation is provided under different control parameters. Fig. 12 shows results with different k_P and the same k_Q. It can be seen that the desirable control performance can be achieved as long as k_P is within the proposed region. However, the system dynamic is too slow when k_P is lower than the proposed region [1, 19.9], and a higher k_P can cause an unacceptable frequency deviation. Fig. 13 shows results with different k_Q and the same k_P. It can be seen that power control performance is satisfied as long as k_Q is within the proposed region. When k_Q is smaller than the region [1e4, 5e5], the system dynamic cannot be ensured. Also, the voltage drop is out of the maximum voltage deviation limitation if k_Q is higher than the proposed region. It can be seen that the desirable control performance can be achieved as long as the parameters are within the proposed region, which agrees with the small signal stability analysis in Section IV.

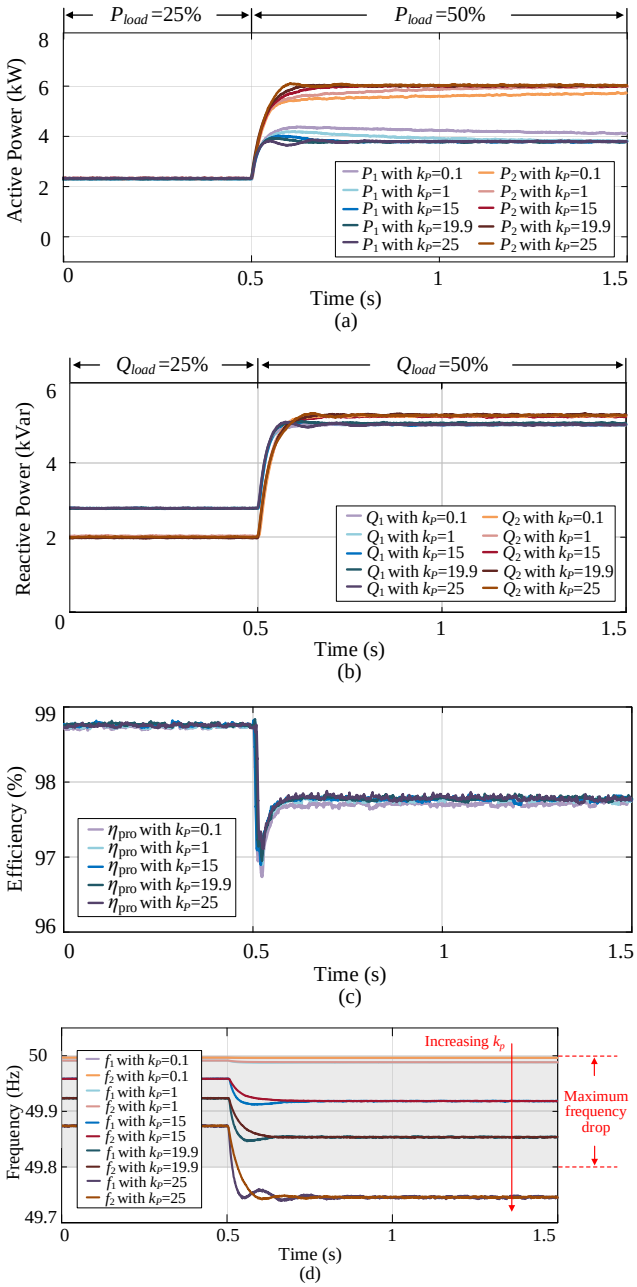

Fig. 12. Simulation results under proposed droop controller with different k_P and the same k_Q (k_Q=2e5). (a) Active power sharing. (b) Reactive power sharing. (c) System efficiency. (d) Frequencies of inverters.

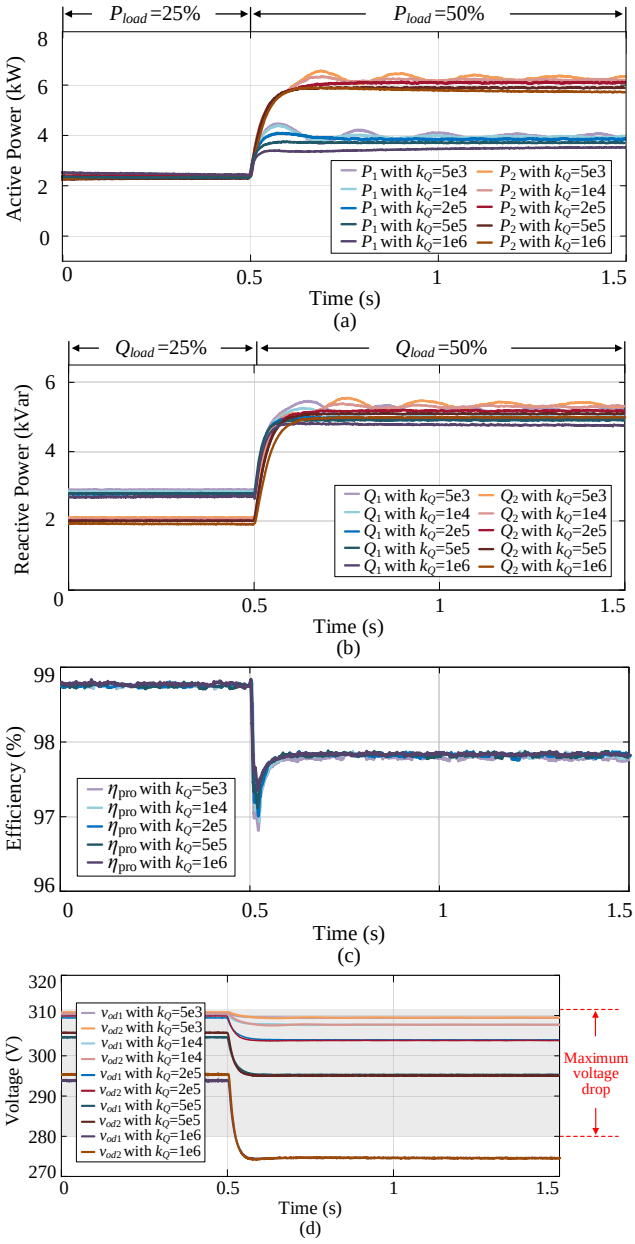

Fig. 13. Simulation results under proposed droop controller with different k_Q and the same k_P (k_P=15). (a) Active power sharing. (b) Reactive power sharing. (c) System efficiency. (d) Output voltage amplitudes of inverters.

Case IV: Inverters with different power ratings

Fig. 14 shows simulation results of paralleled inverters with different power devices (FS6R06VE3_B2 and SK30GD066ETp). Time-varying load is exerted as 10% system capacity during 0-0.5s, 20% system capacity during 0.5-1s, 50% system capacity during 1-1.5s and 80% system capacity during 1.5-2s. Fig. 14 (a)-(d) show power sharing characteristics under conventional droop control strategy and proposed efficiency-prioritized droop control strategy. Fig. 14(e) shows adaptive impedance compensation values. And Fig. 14 (f) shows the compared system efficiency under conventional droop control strategy and proposed droop control strategy. The efficiency improvement results are given in Table II. It can be seen that the proposed droop control method is able to improve system efficiency under different load profiles, which agrees with theoretical analysis shown in Fig. 5 and Fig. 7.

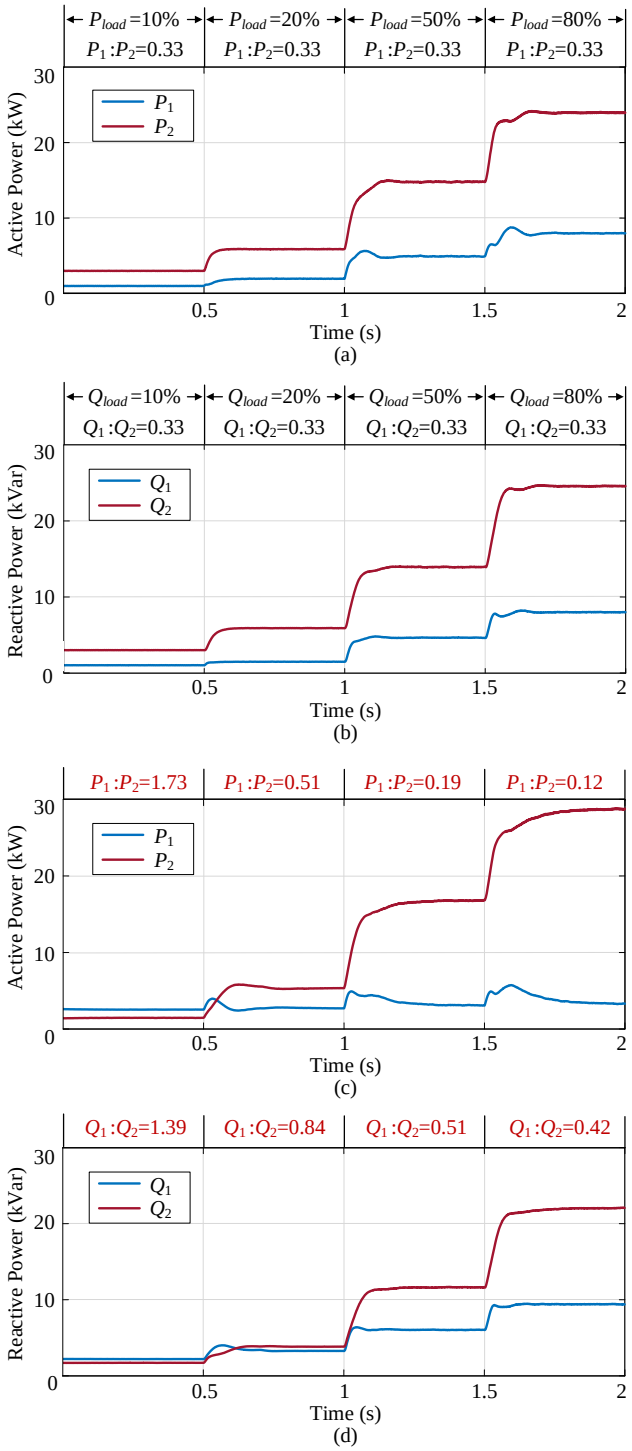

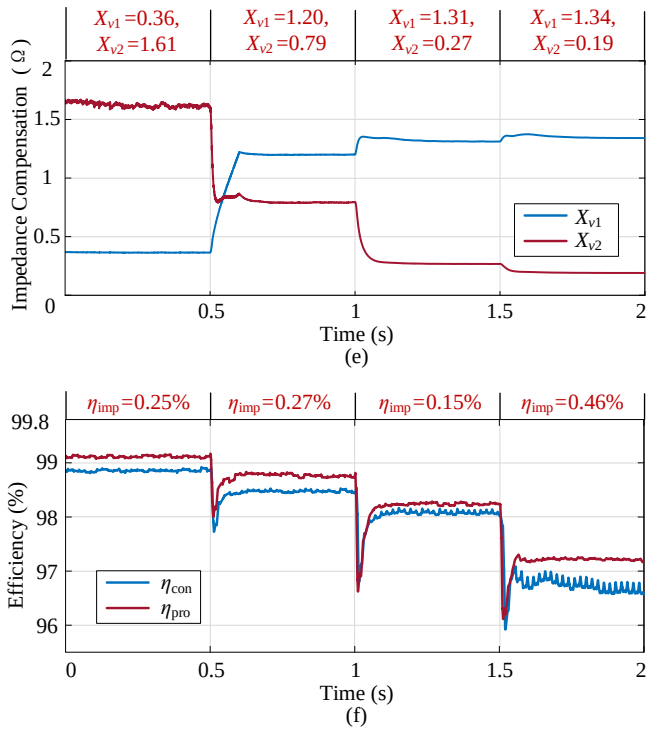

Fig. 14. Simulation results of case IV. (a) Active power sharing under conventional droop control strategy. (b) Reactive power sharing under conventional droop control strategy. (c) Active power sharing under proposed droop control strategy. (d) Reactive power sharing under proposed droop control strategy. (e) Dynamic impedance compensation values. (f) System efficiency under conventional and proposed droop control strategy.

VI. Experimental Verification

To further validate effectiveness of the proposed droop control strategy, experimental verification is implemented in a scaled-down islanded microgrid with two inverters. The circuit diagram of exemplified microgrid is shown in Fig. 1. The scaled-down prototype is shown in Fig. 15, which is controlled by dSPACE 1006. Experiment parameters are given in Table III. Inverters with same power ratings but different power devices are used to validate efficiency improvement performance of the proposed droop controller.

Experimental data of power loss of two inverters under a constant reactive power load (Q_{load}=200Var) is shown in Fig. 16 and fitted power loss coefficients of two inverters are given in Table III. Fig. 17 shows theoretical system efficiency curves of the exemplified microgrid under conventional and proposed droop control strategy. Also, the theoretical improved efficiency is shown in Fig. 17 as the green curve.

Fig. 18 shows experimental results about output currents (Phase A) of paralleled inverters under the proposed efficiency-prioritized droop control strategy. It can be seen that power sharing ratio is dynamically turned to capture optimum efficiency as variation of load profiles. The experimental data of improved efficiency is given in Table IV. It can be seen that the proposed efficiency-prioritized droop control strategy can improve overall efficiency of microgrid within a wide load profile. Also, experimental data in Table IV agrees with the theoretical analysis shown in Fig. 17, which verifies that the proposed efficiency analysis model is able to reveal the time-varying efficiency characteristic and capture optimum efficiency points.

Fig. 19 shows experimental results with load step to validate transient performance of the proposed droop controller. Fig. 19(a) shows output currents (Phase A) of paralleled inverters after load is increased, where the current of inverter1 (light blue curve) is increased after load step to balance load demand and power sharing is adaptively regulated according to load profiles. And Fig. 19(b) shows output currents (Phase A) of paralleled inverters after load is decreased. It can be seen from Fig. 19 that desirable dynamic responses are performed under both increased or decreased load step with the proposed droop control strategy.

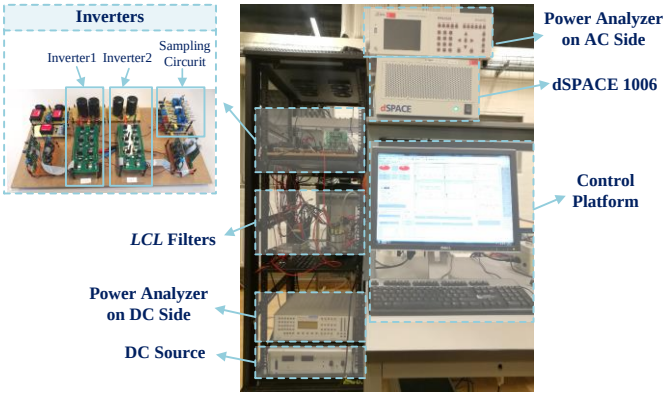

Fig. 15. Photo of experimental setup.

TABLE III
System Parameters in Experiment

Inverter Parameters			
Power device	IGBT	Inverter1 IRG4BH20K-SPbF	Inverter2 IXYP30N120C3
	Diode	STTH1512	STTH1512
DC voltage		V_{dc1}=200V	V_{dc2}=200V
Fitted power loss coefficients		a_1=1.75e-5 b_1=8.58e-2 h_1=10.05	a_2=9.58e-5 b_2=4.50e-2 h_2=6.26

Circuit and Control Parameters			
Filter parameters	L_{f1}=1.8mH C_{f1}=25μF L_{f2}=1.5mH C_{f2}=25μF	Phase voltage frequency reference	V_m^*=311V ω^*=100π rad/s
Line impedance	Z_{l1}=(0.01+j0.63) Ω Z_{l2} = (0.02+j1.26) Ω	Switching frequency	f_{sw1}= f_{sw2}= f_{sw3}=10kHz
Adaptive droop coefficient	k_P=15	Impedance compensation coefficient	k_Q=2e5

TABLE IV
Results About Improved Efficiency in Experiment

Load Profiles (W)	280	330	380	430	500
η_{imp} (%)	0.19	0.08	0.02	0.05	0.23

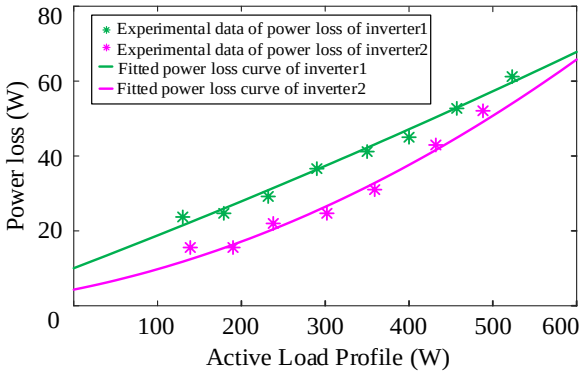

Fig. 16. Experimental data and fitted curves of power loss of two inverters.

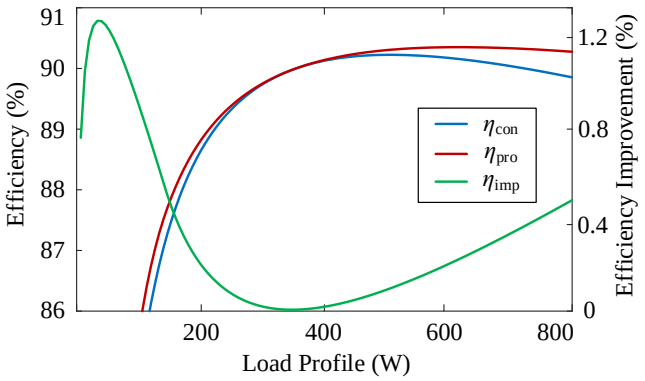

Fig. 17. Theoretical system efficiency curves and efficiency improvement curve.

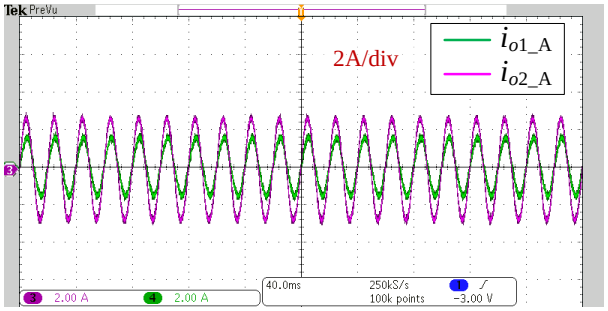

(a)

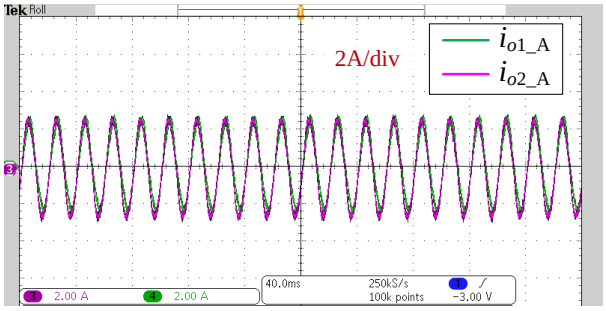

(b)

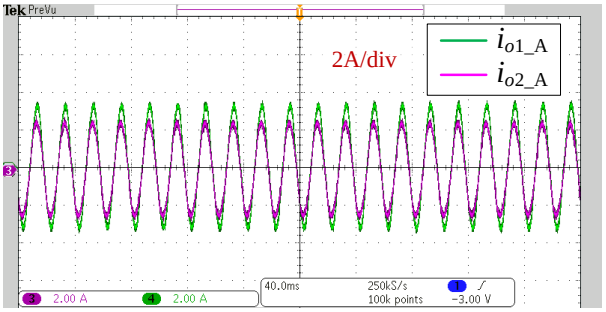

(c)

Fig. 18. Experimental results under the proposed efficiency-prioritized droop control strategy. (a) Output currents (Phase A) of paralleled inverters as P_{load}=280W. (b) Output currents (Phase A) of paralleled inverters as P_{load}=380W. (c) Output currents (Phase A) of paralleled inverters as P_{load}=500W.

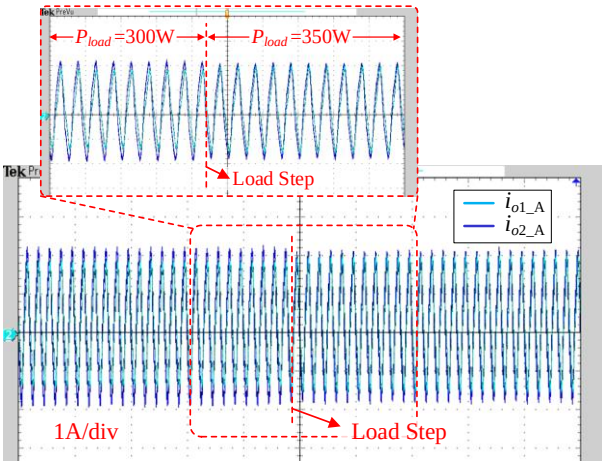

(a)

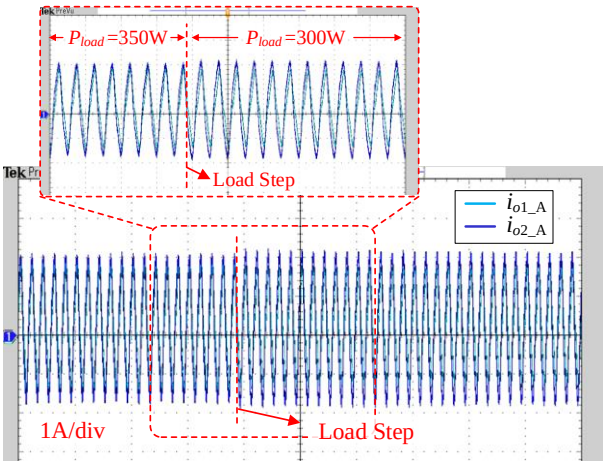

(b)

Fig. 19. Experimental results with load step under the proposed efficiency-prioritized droop control strategy. (a) Output currents (Phase A) of paralleled inverters with increased load. (b) Output currents (Phase A) of paralleled inverters with decreased load.

VII. Conclusions

This paper presents an efficiency-prioritized droop control strategy to improve operation efficiency of microgrids under different load profiles. Efficiency model is first established to analyze time-varying efficiency characteristic under different load profiles. And optimum operation conditions of efficiency model are derived by Lagrange Multiplier Method, which reveals the relationship of optimum efficiency and active/reactive power sharing. Then, the efficiency-prioritized droop control strategy with dynamic impedance compensation loop is developed to improve operation efficiency according to established efficiency model. Small signal stability analysis shows that parameters of the proposed controller have significant influence on system stability, and the guideline for control parameters is formulated. Simulation and experimental results are given to validate the proposed efficiency analysis method and efficiency-prioritized droop control strategy. The verification results show that the proposed efficiency analysis model is able to investigate the time-varying efficiency characteristic and obtain optimum efficiency points. The proposed efficiency-prioritized droop control strategy thus can improve overall efficiency of microgrid under different load profiles.

Appendix

Taking a microgrid with two paralleled inverters as an example, parameter matrixes in (21) are given as (25)-(27), where v_{odi_0} and v_{oqi_0} are stable-state values of output voltage in individual *dq* frame of the *i*-th inverter [34]. v_{pD_0} and v_{pQ_0} are stable-state values of common bus voltage in common *DQ* frame [34]. $\delta_{i\_\mathrm{frame}}$ is the angle between the reference frame of *i*-th inverter and the common reference frame [34].

$$A=\begin{bmatrix} A_{INV}+B_{INV}M_{INV}C_{INVc} & B_{INV}M_{1line} & 0_{10\times 2} \\ B_{1line}M_{INV}C_{INVc}+B_{3line}C_{INV\omega} & A_{line}+B_{1line}M_{1line}+B_{2line}M_{2line} & B_{2line}M_{load} \\ B_{2load}C_{INV\omega} & B_{1load}M_{2line} & A_{load}+B_{1load}M_{load} \end{bmatrix} \tag{25}$$

$$\begin{cases} A_{INV}=A_{INV1}+B_{\omega com}C_{INV\omega} \\ where \\ A_{INV1}=\begin{bmatrix} A_{inv1} & 0_{5\times 5} \\ 0_{5\times 5} & A_{inv2} \end{bmatrix},\ A_{invi}=\begin{bmatrix} A_{1Pi} & A_{2Pi} \\ A_{1Ci}+\begin{bmatrix} B_{1Ci}T_{Vi}^{-1} & 0_{2\times 1} & 0_{2\times 1} \end{bmatrix} & A_{2Ci} \end{bmatrix}, \\ A_{1Pi}=\begin{bmatrix} 0 & -2k_Pa_i & -k_Pe_i \\ 0 & -\omega_c & -\omega_c n_i i_{odi\_0} \\ 0 & \omega_c K_{X_{vi}\_P_i}\left(i_{odi\_0}^2+i_{oqi\_0}^2\right) & -\omega_c-\omega_c n_i i_{oqi\_0}+\omega_c K_{X_{vi}\_Q_i}\left(i_{oqi\_0}^2+i_{odi\_0}^2\right) \end{bmatrix} \\ A_{2Pi}=\begin{bmatrix} 0 & 0 \\ -X_{vi\_0}\omega_c i_{oqi\_0}+\omega_c v_{odi\_0} & X_{vi\_0}\omega_c i_{odi\_0}+\omega_c v_{oqi\_0} \\ X_{vi\_0}\omega_c i_{odi\_0}-\omega_c v_{oqi\_0} & X_{vi\_0}\omega_c i_{oqi\_0}+\omega_c v_{odi\_0} \end{bmatrix} \\ A_{1Ci}=\frac{1}{L_{fi}}\begin{bmatrix} 0 & K_{X_{vi}\_P_i}i_{oqi\_0} & K_{X_{vi}\_Q_i}i_{oqi\_0}-n_i \\ 0 & -K_{X_{vi}\_P_i}i_{odi\_0} & -K_{X_{vi}\_Q_i}i_{odi\_0} \end{bmatrix},\ A_{2Ci}=\frac{1}{L_{fi}}\begin{bmatrix} 0 & \omega_{i\_0}L_{fi}+X_{vi\_0} \\ -\omega_{i\_0}L_{fi}-X_{vi\_0} & 0 \end{bmatrix} \\ B_{1Ci}=-\frac{1}{L_{fi}}\begin{bmatrix} 1 & 0 \\ 0 & 1 \end{bmatrix},\ T_{Vi}^{-1}=\begin{bmatrix} -v_{pD\_0}\sin\left(\delta_{i\_\mathrm{frame}}\right)+v_{pQ\_0}\cos\left(\delta_{i\_\mathrm{frame}}\right) \\ -v_{pD\_0}\cos\left(\delta_{i\_\mathrm{frame}}\right)-v_{pQ\_0}\sin\left(\delta_{i\_\mathrm{frame}}\right) \end{bmatrix} \\ B_{\omega com}=\begin{bmatrix} B_{\omega com1} \\ B_{\omega com2} \end{bmatrix},\ B_{\omega comi}=\begin{bmatrix} -1 & 0_{1\times 4} \end{bmatrix}^T \\ C_{INV\omega}=\begin{bmatrix} 0 & -2k_Pa_1 & -k_Pe_1 & 0_{1\times 7} \end{bmatrix} \end{cases} \tag{26}$$

$$\begin{cases} B_{INV}=\begin{bmatrix} B_{inv1} & 0_{5\times2} \\ 0_{5\times2} & B_{inv2} \end{bmatrix} \\ where \\ B_{invi}=\begin{bmatrix} 0_{3\times2} \\ B_{1Ci}T_{Si}^{\ -1} \end{bmatrix}, T_{Si}=\begin{bmatrix} \cos\left(\delta_{i\_frame}\right) & -\sin\left(\delta_{i\_frame}\right) \\ \sin\left(\delta_{i\_frame}\right) & \cos\left(\delta_{i\_frame}\right) \end{bmatrix} \end{cases} \quad \begin{cases} C_{INVc}=\begin{bmatrix} C_{invc1} & 0_{2\times5} \\ 0_{2\times5} & C_{invc2} \end{bmatrix} \\ where \\ C_{invci}=\begin{bmatrix} T_{Ci} & 0_{2*1} & 0_{2*1} & T_{Si} \end{bmatrix}, \\ T_{Ci}=\begin{bmatrix} -i_{odi\_0}\sin\left(\delta_{i\_frame}\right)-i_{oqi\_0}\cos\left(\delta_{i\_frame}\right) \\ i_{odi\_0}\cos\left(\delta_{i\_frame}\right)-i_{oqi\_0}\sin\left(\delta_{i\_frame}\right) \end{bmatrix} \end{cases}$$

$$\begin{cases} B_{1line}=\begin{bmatrix} B_{1line1} & 0_{2*2} \\ 0_{2*2} & B_{1line2} \end{bmatrix} \\ where \\ B_{1linei}=\dfrac{1}{L_{linei}}\begin{bmatrix} 1 & 0 \\ 0 & 1 \end{bmatrix} \end{cases} \quad \begin{cases} B_{2line}=\begin{bmatrix} B_{2line1} \\ B_{2line2} \end{bmatrix} \\ where \\ B_{2linei}=-\dfrac{1}{L_{linei}}\begin{bmatrix} 1 & 0 \\ 0 & 1 \end{bmatrix} \end{cases} \quad \begin{cases} B_{3line}=\begin{bmatrix} B_{3line1} \\ B_{3line2} \end{bmatrix} \\ where \\ B_{3linei}=\begin{bmatrix} i_{lineQi\_0} \\ -i_{lineDi\_0} \end{bmatrix} \end{cases} \quad \begin{cases} B_{1load}=\dfrac{1}{L_{load}}\begin{bmatrix} 1 & 0 \\ 0 & 1 \end{bmatrix} \\ B_{2load}=\begin{bmatrix} i_{loadQ\_0} \\ -i_{loadD\_0} \end{bmatrix} \end{cases} \tag{27}$$

$$\begin{cases} M_{INV}=\begin{bmatrix} R_N & 0 & 0 & 0 \\ 0 & R_N & 0 & 0 \\ 0 & 0 & R_N & 0 \\ 0 & 0 & 0 & R_N \end{bmatrix}, M_{1line}=-M_{INV}, M_{2line}=\begin{bmatrix} R_N & 0 & R_N & 0 \\ 0 & R_N & 0 & R_N \end{bmatrix}, M_{load}=\begin{bmatrix} -R_N & 0 \\ 0 & -R_N \end{bmatrix} \end{cases}$$

REFERENCES

[1] R. Lasseter, "Smart distribution: Coupled microgrids," *Proc. IEEE*, vol. 99, no. 6, pp. 1074-1082, Jun. 2011.

[2] P. Lin, C. Jin, J. Xiao, X. Li, D. Shi, Y. Tang, and P. Wang, "A distributed control architecture for global system economic operation in autonomous hybrid AC/DC microgrids," *IEEE Trans. Smart Grid*, vol. 10, no. 3, pp. 2603-2617, May 2019.

[3] Y. Wang, X. Wang, F. Blaabjerg, and Z. Chen, "Harmonic instability assessment using state-space modeling and participation analysis in inverter-fed power system," *IEEE Trans. Ind. Electron.*, vol. 64, no. 1, pp. 806-816, Jan. 2017.

[4] P. Lin, T. Zhao, B. Wang, Y. Wang, and P. Wang, "A semi-consensus strategy toward multi-functional hybrid energy storage system in DC microgrids," *IEEE Trans. Energy Convers.*, early access, 2019. Doi: 10.1109/TEC.2019.2936120.

[5] C. Fei, Q. Li, and F. C. Lee, "Digital implementation of light-load efficiency improvement for high-frequency LLC converters with simplified optimal trajectory control," *IEEE J. Emerg. Sel. Topics Power Electron.*, vol. 6, no. 4, pp. 1850-1859, Dec. 2018.

[6] F. Deng, Q. Wang, D. Liu, Y. Wang, M. Cheng, and Z. Chen, "Reference submodule-based capacitor monitoring strategy for modular multilevel converters," *IEEE Trans. Power Electron.*, vol. 34, no. 5, pp. 4711-4721, May 2019.

[7] Z. Tang, M. Su, Y. Sun, B. Cheng, Y. Yang, F. Blaabjerg, and L. Wang, "Hybrid UP-PWM scheme for HERIC inverter to improve power quality and efficiency," *IEEE Trans. Power Electron.*, vol. 34, no. 5, pp. 4292-4303, May 2019.

[8] Z. Tang, Y. Yang, M. Su, T. Jiang, F. Blaabjerg, H. Dan, and X. Liang, "Modulation for the AVC-HERIC inverter to compensate for deadtime and minimum pulse width limitation distortions," *IEEE Trans. Power Electron.*, vol. 35, no. 3, pp. 2571-2584, Mar. 2020.

[9] Y. Qin, Y. Yang, S. Li, Y. Huang, S.-C. Tan and S. Hui, "A high efficiency DC/DC converter for high voltage gain high current applications," *IEEE J. Emerg. Sel. Topics Power Electron.*, early access, 2019. Doi: 10.1109/JESTPE.2019.2908416.

[10] B. Jin and X. Yuan, "Topology, efficiency analysis, and control of a four-level π-type converter," *IEEE J. Emerg. Sel. Topics Power Electron.*, vol. 7, no.2, pp. 1044-1059, Jun. 2019.

[11] Z. Xin, X. Wang, P. C. Loh, and F. Blaabjerg, "Grid-current-feedback control for LCL-filtered grid converters with enhanced stability," *IEEE Trans. Power Electron.*, vol. 32, no.4, pp. 3216-3228, Jun. 2016.

[12] D. Thenathayalan, L. Chun-gu, and P. Joung-hu, "High-order resonant converter topology with extremely low-coupling contactless transformers," *IEEE Trans. Power Electron.*, vol. 31, no. 3, pp. 2347-2361, Mar. 2016.

[13] H. Wang, A. M. Khambadkone, and X. Yu. "Control of parallel connected power converters for low voltage microgrid-Part II: Dynamic electro-thermal modeling." *IEEE Trans. Power Electron.*, vol. 25, no. 12, pp. 2971-2980, Dec. 2010.

[14] X. Yu, A. M. Khambadkone, H. Wang, and S. T. S. Terence. "Control of parallel connected power converters for low voltage microgrid-Part I: A hybrid control architecture." *IEEE Trans. Power Electron.*, vol. 25, no. 12, pp. 2962-2970, Dec. 2010.

[15] P. Bartal and I. Nagy, "Game theoretic approach for achieving optimum overall efficiency in DC/DC converters," *IEEE Trans. Ind. Electron.*, vol. 61, no. 7, pp. 3202-3209, Jul. 2014.

[16] S. Wang, J. Liu, Z. Liu, T. Wu, and B. Liu. "Efficiency-based optimization of steady-state operating points for parallel source converters in stand-alone power system." In *Proc. 8th ECCE Asia*, May. 22-26, 2016, pp. 163-170.

[17] Y. Wang, D. Liu. Z. Chen. and P. Liu, "A hierarchical control strategy of microgrids toward reliability enhancement," In *Proc. IEEE icSmartGrid*, Dec. 4-6, 2018, pp. 123-128.

[18] R. Razi, H. Iman-Eini, and M. Hamzeh, "An impedance-power droop method for accurate power sharing in islanded resistive microgrids," *IEEE J. Emerg. Sel. Topics Power Electron.*, early access, 2019. Doi: 10.1109/JESTPE.2019.2926319.

[19] Y. Wang, X. Wang, Z. Chen, and F. Blaabjerg, "Distributed optimal control of reactive power and voltage in islanded microgrids," *IEEE Trans. Ind. Applicat.*, vol. 53, no.1, pp. 340-349, Feb. 2017.

[20] L. Meng, T. Dragicevic, J. C. Vasquez, and J. M. Guerrero, "Tertiary and secondary control levels for efficiency optimization and system

damping in droop controlled DC-DC converters," *IEEE Trans. Smart Grid.*, vol. 6, no.6, pp. 2615-2626, Jun. 2015.
[21] J.-H. Teng, S.-H. Liao, W.-H. Huang, and C.-C. Chiang, "Smart control strategy for conversion efficiency enhancement of parallel inverters at light loads," *IEEE Trans. Ind. Electron.*, vol. 63, no. 12, pp. 7586–7596, Dec. 2016.
[22] G. Chen and X. Cai, "Adaptive control strategy for improving the efficiency and reliability of parallel wind power converters by optimizing power allocation," *IEEE Access*, vol. 6, pp. 6138–6148, Jan. 2018.
[23] X. Hou, Y. Sun, X. Zhang, J. Lu, P. Wang, and J. M. Guerrero, "Improvement of frequency regulation in VSG-based AC microgrid via adaptive virtual inertia," *IEEE Trans. Power Electron.*, vol.35, no.2, pp.1589-1602, Feb. 2020.
[24] W. Yuan, Y. Wang, X. Ge, X. Hou, and H. Han, "A unified distributed control strategy for hybrid cascaded-parallel microgrid," *IEEE Trans. Energy Convers.*, vol. 34, no. 4, pp. 2029-2040, Dec. 2019.
[25] X. Hou, Y. Sun, H. Han, Z. Liu, W. Yuan, M. Su, "A fully decentralized control of grid-connected cascaded inverters," *IEEE Trans. Sustainable Energy*, vol. 10, pp.315-317, Jan. 2019.
[26] Y. Wang, Z. Chen, X. Wang, Y. Tian, Y. Tan, and C. Yang, "An estimator-based distributed voltage predictive control strategy for AC islanded microgrids," *IEEE Trans. Power Electron.*, vol. 30, no. 7, pp. 3934-3951, July. 2015.
[27] L. Meng, T. Dragicevic, J. M. Guerrero, and J. C. Vasquez, "Dynamic consensus algorithm based distributed global efficiency optimization of a droop controlled DC microgrid," in *Proc. IEEE Int. Energy Conf. (ENERGYCON)*, May 2014, pp. 1276-1283.
[28] W. Yuan, Y. Wang, D. Liu, and F. Deng, "Adaptive droop control strategy of autonomous microgrid for efficiency improvement," in *Proc. PEDG*, Jun. 3-6, 2019, pp. 972-977.
[29] M. C, Chandorkar, D. M. Divan, and R. Adapa, "Control of parallel connected inverters in standalone ac supply systems," *IEEE Trans. Ind. Appl.*, vol.29, no.1, pp.136-143, Jan.1993.
[30] W. Yuan, Y. Wang, D. Liu, F. Deng, and Z. Chen, "Robust droop control of AC microgrid against nonlinear characteristic of inductor," in *Proc. PEDG*, Jun. 3-6, 2019, pp. 642-647.
[31] Y. Wang, D. Liu, P. Liu, F. Deng, D. Zhou, and Z. Chen, "Lifetime-oriented droop control strategy for AC islanded microgrids," *IEEE Trans. Ind. Appl.*, vol. 55, no. 3, pp. 3252-3263, Feb. 2019.
[32] Y. Wang, X. Wang, Z. Chen, and F. Blaabjerg, "Small-signal stability analysis of inverter-fed power systems using component connection method," *IEEE Trans. Smart Grid*, vol. 9, no. 5, pp. 5301-5310, Sep. 2018.
[33] E. A. A. Coelho, P. C. Cortizo, and P. F. D. Garcia, "Small-signal stability for parallel-connected inverters in stand-alone AC supply systems," *IEEE Trans. Ind. Appl.*, vol. 38, no. 2, pp. 533-542, Mar. 2002.
[34] N. Pogaku, M. Prodanovic, and T. C. Green, "Modeling, analysis and testing of autonomous operation of an inverter-based microgrid," *IEEE Trans. Power Electron.*, vol. 22, no. 2, pp. 613-625, Mar. 2007.
[35] "IGBT modules technical information," FS6R06VE3_B2, *Infineon datasheet*, 2013.
[36] "IGBT modules technical information," SKiiP 01NEC066V3, *Semikron datasheet*, 2009.
[37] "IGBT modules technical information," SK30GD066ETp, *Semikron datasheet*, 2015.

Wenbin Yuan received the B.Eng. degree from Xiangtan University, Xiangtan, China, in 2015, and M.Sc. degree from the School of Information Science and Engineering, Central South University, Changsha, China, in 2018.

Currently, he is working toward Ph.D. degree in the Department of Energy Technology, Aalborg University, Denmark. His research interests include distributed power generation system, microgrid, as well as control technologies of power electronic-dominated power system.

Yanbo Wang (S'15-M'17-SM'19) received Ph.D. degree in the Department of Energy Technology, Aalborg University, Denmark, in 2017. Currently, he is with the Department of Energy Technology in Aalborg University as an Assistant Professor. From June to October of 2016, he was a visiting scholar in Power System Research Group of the Department of Electrical and Computer Engineering, University of Manitoba, Winnipeg, MB, Canada. His research interests include distributed power generation system, wind power system, microgrid, as well as operation and control technologies of power electronic-dominated power system.

Dr. Wang's paper on Distributed Power System received the First Prize Paper Award of the 6th International Conference of Smart Grid cosponsored by IEEE Industry Application Society in 2018. He received the Best Session Paper Award at the annual conference of the IEEE Industrial Electronics Society in 2015 in Japan.

Dong Liu (S'15-M'18-SM'19) received the B.Eng. and M.Sc. in electrical engineering from South China University of Technology, Guangzhou, China, in 2008 and 2011, and the Ph.D. degree in energy technology from the Department of Energy Technology, Aalborg University, Aalborg, Denmark, in 2018. Currently, he is with the Department of Energy Technology in Aalborg University as a Postdoctoral Researcher.

From 2011 to 2014, he was an R&D engineer in Emerson Network Power Co., Ltd., Shenzhen, China. From May, 2017 to November, 2017, he was a visiting scholar at Center for Power Electronics Systems (CPES), Virginia Tech, Blacksburg, VA, USA. His main research interests include the modeling and control of power electronics converters, high-efficiency power conversion systems, and power electronics applications in renewable energy power generations.

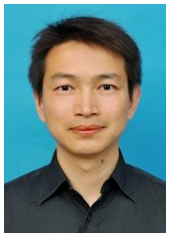

Fujin Deng (SM'19) received the B.Eng. degree in Electrical Engineering from China University of Mining and Technology, Jiangsu, China, in 2005, the M.Sc. degree in Electrical Engineering from Shanghai Jiao Tong University, Shanghai, China, in 2008, and the Ph.D. degree in Energy Technology from the Department of Energy Technology, Aalborg University, Aalborg, Denmark, in 2012.

He joined the Southeast University in 2017 as a Professor in the School of Electrical Engineering, Southeast University, Nanjing, China. From 2013 to 2015 and from 2015 to 2017, he was a Postdoctoral Researcher and an Assistant Professor, respectively, in the Department of Energy Technology, Aalborg University, Aalborg, Denmark. His main research interests include wind power generation, multilevel converters, high-voltage direct-current technology, DC grid and offshore wind farm-power systems dynamics.

Zhe Chen (M'95-SM'98-F'18) received the B.Eng. and M.Sc. degrees from Northeast China Institute of Electric Power Engineering, Jilin City, China, and the Ph.D. degree from University of Durham, U.K.

Dr. Chen is a full Professor with the Department of Energy Technology, Aalborg University, Denmark. He is the leader of Wind Power System Research program at the Department of Energy Technology, Aalborg University and the Danish Principle Investigator for Wind Energy of Sino-Danish Centre for Education and Research. His research areas are power systems, power electronics and electric machines, and his main current research interests are wind energy and modern power systems. He has led many research projects and has more than 500 publications in his technical fields.